Dear Renée,

Thank you for your assistance with the paper and giving it a close read yourself. I've made the changes recommended in the editorial notes and most of those in the comments. Please see details below.

Thank you,

Steve Kidder

Editorial notes (need to be corrected or resolved):

Page 1 - line 18 - Please capitalize "moho"

> Changed

starting from Page 2 - line 33 - In running text, please consistently use "Fig." - not "Figure".

> OK, Hopefully I did this correctly. I changed both instances in parentheses and also those in the main text for single and plural to "Fig." For example, "This is demonstrated in Fig. 3, but also seen elsewhere (e.g. Fig. 5, 6, 7)"

Page 3 - line 30 - one space too many after end of sentence

> Done

Page 4 - line 30 - one space too many after end of sentence

> Done

Page 4 - line 35 - Could you be a bit more specific as to how you define and determine "grain size" ?

> Yes. We added the following sentence to the last paragraph of the methods section: "Grains were distinguished from subgrains based on the sharpness of grain boundaries under cross-polarized light."

Page 5 - line 18 - It would be important to know what is the grain size here, in a case where you have elongated grains. In Fig.3 and Fig.4c, you may want to specify "long diameter" or "equivalent diameter" or whatever it is...

We added the following sentence to the last paragraph of the methods section: "Long and short axes of elongate grains were measured, and reported sizes for these grains are diameters of circles with the same area as an ellipse having the measured axes lengths."

Page 5 - line 33 - Much as I look at Fig.4a and 4b. The rims look bright to me (as they should, being depleted) - not dark. Also, please refer to both Fig.4a and 4b.

We agree, the rims in figure 4 are bright. But the image in figure 4a and 4b are not "typical" CL images, they are the hyperspectral CL images (which we wanted to show for other reasons…).

We've added information explaining this explicitly now: "Typical CL images of the Alpine Fault mylonites and protomylonites show a homogeneous illumination (e.g. Fig. 4a), generally with a thin dark rim around the edges of grains (note that this relationship is reversed in the hyperspectral CL images in Fig. 4a and 4b that show brighter rims).

Page 7 - line 37 - Please use Ga instead of byr.

Fixed

Page 21 - Figure 4 - Why did you use uppercase A,B,C,D while references to image are lowercase? I am not sure if Solid Earth has a policy about using upper- or lowercase.

We're confused here. We did refer to the images in the figure caption using uppercase, i.e. the same as is shown in the upper corners of the figures. For example the caption says "…in panels (B) and (D)…"

Page 21 - line 6 - Figure 4 – caption - As Fig.4d show a cross-polarized photomicrograph (...), the observation that "grains with c-axes oriented perpendicular to the plane of the section are dark in panels (B) and (D)" cannot strictly be upheld. Whether or not a grain appears dark on a cross- polarized photomicrograph not only depends on the inclination of the quartz c-axis w/ r to the image plane, but also on the orientation w/r to the horizontal and vertical direction within the image plane. In fact you also find dark grains in Fig. 4d that are not dark in Fig. 4d. If you had used circular polarization, the correlation between Fig. 4b and 4d would be perfect.Please modify or delete this remark from the caption.

Thanks for the information on circular polarizers. I'd like to get one. We rephrased it in a way that is actually true: "The blue spectrum peak (~470 nm, 2.65 eV) is dependent on quartz c-axis orientation, since dark grains in panel (B) are also dark in panel (D)."

Page 22 - line 3 - Figure 5 - "The data are jittered along the x axis to increase visibility." As you are plotting Ti concentrations in quartz vs. the distance, this sentence makes no sense here. Please delete.

>This comment was also sent in a follow up email:

After I pressed the submit button, I suddenly realized that I had misunderstood something w/r to your your Figures 5 7 and 9 (you'll see when you read my comments). In the captions of those figures, you wrote that the data are jittered. I could not understand why you would want to mention this - I thought you could just see it. I thought that you had plotted the data at distances measured in the field.. And therefore I wrote in my review that this comment was unnecessary Now it occurs to me that maybe the distances of the data points are not measured (or calculated) actual distances, but approximate distances typical of 4 or so separate horizons?

So instead of removing the sentence you could maybe clarify that the jittering is introduced "artificially"...? (Maybe I am not the only one to get it wrong...)

Most of the data (>90% I think), is from one transect. There are ~15 locations along this transect, so a lot of the data would plot on top of each other at the different localities. What we have done is shift the plotted distance values from their true values by adding some random noise (jittering) to the measured distance values. Without doing this, the trends and concentrations of data can't be seen well. Since this wasn't clear, we've replaced the sentence with "The data are jittered along the x axis by an amount not exceeding 30 km in order to increase the visibility of the data." Hopefully this is clearer.

Page 22 - line 11 Figure 6.No, you are not plotting "grain size vs. Ti concentration" but the reverse. One always plots Y against X (where X is the independent variable and usually the horizontal), Please correct.

This has been corrected.

Page 23 Figure 7 (cf. Figure 4). Why did you use uppercase A,B while references to image are lowercase? I am not sure if Solid Earth has a policy about using upper- or lowercase.

This is strange. In the version we have and the most recent one online (se-2018-12-manuscript-version2.pdf), we didn't do that. The figure captions use upper case references, e.g. "Data from Cross et al. (2015) are plotted in panel A but are not available for panel B" and "The lack of a clear trend in (B)"

Page 23 - line 13 Figure 7 (cf. Figure 5)"The data are jittered along the x axis to increase visibility."Again, as you are ostensibly plotting Ti concentrations in quartz vs. the distance, this sentence makes no sense here.Please delete

> We've changed it to "The data are jittered along the x axis in order to increase visibility."

Page 24 - line 11 Figure 8 Again, you are not plotting "grain size vs. Ti concentration" but the reverse. (see Fig. 6)Please correct.

> This has been corrected.

Page 25 - line 11Figure 9"Data are jittered along the x-axis."Same as in Figure caption 7, this sentence makes no sense here. Please delete.Instead, please comment on the inset.

> Now changed to "The data are jittered along the x axis by an amount not exceeding 50 km in order to increase visibility."

Page 26 - line 4 Figure 10 "Image" ? Please specify.

> Replaced "image" with "photomicrograph"

Comments (respond at your own discretion):

Page 1 line 31 - you say "...where the examination of plate boundary phenomena ... can be informed by observation ...."getting close to Yogi Berra's famous quote: "You can observe a lot by just watching." :-)

> True. We changed it to "the understanding of…" rather than "examination of"

Page 2 - line 30 - you say: "classic sequence of fault rocks: protomylonites, mylonites, ultramylonites, and finally cataclasites" - cataclasites are "classical" if the fault development is following a cooling path or later-stage brittle overprint....

> Unchanged

Page 3 - line 3 - your write: "clockwise rotation (when viewed from the SW) and dextral shearing..." - I am not familiar with the details of the Alpine fault deformational history... So I wonder: are "clockwise rotation" and "dextral shearing" two different events or both the same? Specifying the viewing direction ("when viewed from the SW") indicates to me that the "rotation" must be on a vertical or very steep plane, and presumably applies to the *dextral shearing" too. If so, and if both "clockwise rotation" and "dextral shearing" are the same you might consider calling this " top to the NE shearing" and save yourself the viewing direction...

They are considered to be different things.

Page 3 - line 10 - What is the basis for the strain determinations? Any references ?

Added “based on thickness of offset, mylonitized pegmatite veins (Norris and Cooper, 2003)”

Page 3 - line 38 (Page 4 - line 1) - why "common in either" - why not "common in both" or simply "common in" ?

No good reason. We removed the word “either”

Page 23 - line 10-13 - Figure 7 - Very long caption. "The lack of a clear trend in (B) suggests that..." etc. until "... not available for panel B."You may consider inserting (and possibly shortening) this part of the caption into the running text on page 6 - line 19.

We removed the sentence about panel B.

Page 24 - line 5-11 Figure 8 Very long caption. "Away from the fault this trend..." etc. until "... of fine grains in the ultramylonite."I think it would be better to move this descriptive part of the caption to the running text on page 6 - line 35.

We agree it’s too long. There was also some duplicated information even within the caption. We shortened and edited it to “Figure 8. Ti vs. grain size for Gaunt Creek samples. Samples at structural distances <160 m from the fault are shown in black (mainly ultramylonites), while mylonites and protomylonites are plotted in transparent purple. The trend in the samples close to the fault suggests late recrystallization (as indicated by finer grain size) occurred at conditions where lower concentrations of Ti were stable. Only partial equilibration of Ti-in-quartz values was achieved during recrystallization of fine grains in the ultramylonite. Away from the fault there is not a general trend of fine grains having lower Ti concentrations.”

Page 27 - line 5-10 Figure 11Very long caption. "Ti activity is constrained by the fact that..." etc. until "... as summarized by Toy et al. (2010)."Consider moving this part of the caption to the running text on page 8 - line 9.

Agreed that it’s too long. We removed the sentence “The geothermal gradient proposed here is based on new data indicating mylonite and protomylonite deformation occurred at temperatures from roughly 600 to 450 °C whilst Ti-in-quartz concentrations of ~3 ppm were stable" since this is already clearly stated elsewhere.

Page 28 - Figure 12 In a time where it has become fashionable to attribute every brittle microstructure to an earth quake, I would welcome if you could label the horizontal line in Figure 12 as "limit of seismicity" (as in text) and remove "Earthquakes" and "No Earthquakes". - Else, the next thing you know is somebody citing your paper as a demonstration of earthquakes as producing ultramylonites with low Ti-in-quartz values.

OK, we've made this change.

Constraints on Alpine Fault (New Zealand) Mylonitization Temperatures and Geothermal Gradient from Ti-in-quartz Thermobarometry

Steven B. Kidder[1], Virginia G. Toy[2], David J. Prior[2], Timothy A. Little[3], Ashfaq Khan[1], Colin MacRae[4]

[1]Department of Earth and Atmospheric Science, City College New York, New York, 10031, USA
[2]Department of Geology, University of Otago, Dunedin, New Zealand
[3]School of Geography, Environment and Earth Sciences, Victoria University of Wellington, Wellington, New Zealand
[4]CSIRO Mineral Resources, Microbeam Laboratory, Private Bag 10, 3169 Clayton South, Victoria, Australia

Correspondence to: Steven B. Kidder (skidder@ccny.cuny.edu)

Abstract. We constrain the thermal state of the central Alpine Fault using approximately 750 Ti-in-quartz SIMS analyses from a suite of variably deformed mylonites. Ti-in-quartz concentrations span more than an order of magnitude from 0.24 to ~5 ppm, suggesting recrystallization of quartz over a 300 °C range in temperature. Most Ti-in-quartz concentrations in mylonites, protomylonites, and the Alpine Schist protolith are between 2 and 4 ppm and do not vary as a function of grain size or bulk rock composition. Analyses of 30 large, inferred-remnant quartz grains (>250 µm), as well as late, cross-cutting, chlorite-bearing quartz veins also reveal restricted Ti concentrations of 2-4 ppm. These results indicate that the vast majority of Alpine Fault mylonitization occurred within a restricted zone of pressure-temperature conditions where 2-4 ppm Ti-in-quartz concentrations are stable. This constrains the deep geothermal gradient from the Moho to about 8 km to a slope of 5 °C/km. In contrast, the small grains (10-40 µm) in ultramylonites have lower Ti concentrations of 1-2 ppm, indicating a deviation from the deeper pressure-temperature trajectory during the latest phase of ductile deformation. These constraints suggest an abrupt, order of magnitude change in the geothermal gradient to an average of about 60 °C/km at depths shallower than about 8 km, i.e. within the seismogenic zone. Anomalously, the lowest-Ti quartz (0.24- 0.7 ppm) occurs away from the fault in protomylonites, suggesting that the outer fault zone experienced minor plastic deformation late in the exhumation history when more fault-proximal parts of the fault were deforming exclusively by brittle processes.

Deleted: m

1. Introduction

The Alpine Fault is the major structure of the Pacific-Australian plate boundary through New Zealand's South Island. During dextral reverse fault slip, a <5 million year old, ~1 km thick mylonite zone (e.g. Sibson et al., 1979) was exhumed in the hanging-wall, providing a unique exposure of deep crustal material deformed to very high strains under boundary conditions constrained by present-day plate motions (e.g. Norris and Toy, 2014). The Alpine Fault is thus a rare location where the understanding of plate boundary phenomena such as major earthquakes (Sutherland et al., 2007) or slow slip events (Chamberlain et al., 2014) can be informed by observation of rocks that recently experienced these events. Because rock deformation was recent and continues today, aspects such as total strain and strain rate (Norris and Cooper, 2003), stress levels (Liu and Bird, 2002), exhumation rates (e.g. Little et al., 2005), and depth of seismicity (Leitner. et al., 2001) are known with a relatively high degree of certainty.

Deleted: examination of

One poorly-constrained aspect of Alpine Fault deformation is the temperature distribution at depth along the structure. The geothermal gradient is a key factor in estimating rock strength and the position of the brittle-ductile transition (e.g. Kohlstedt et al., 1995), interpreting exhumation rates based on radiometric ages (e.g. Batt et al., 2000), and setting boundary conditions for thermomechanical models (e.g. Batt and Braun, 1999; Herman et al., 2007) and validating their results. Some constraints on temperature are available for deep levels of the central Alpine Fault (e.g. Holm et al., 1989; Craw, 1997; Vry et al., 2004; Toy et al., 2010; Cross et al., 2015), however estimates of temperature vary significantly, disagreeing by as much as 200 °C at any given depth along the structure (Toy, 2007).

One tool with potential to improve understanding of the temperature distribution along the Alpine Fault is titanium-in-quartz thermobarometry (Wark and Watson, 2006; Thomas et al., 2010). In experiments where quartz is crystallized from a Si- and Ti-saturated aqueous fluid, trace concentrations of Ti-in-quartz are observed to be a function of both temperature and pressure (Thomas et al., 2010; Thomas et al., 2015). In both experimental and natural deformation, Ti concentrations in quartz are often reset during recrystallization (e.g. Kohn and Northrup, 2009; Behr and Platt, 2011; Kidder et al., 2013; Nachlas et al., 2014; Nachlas and Hirth, 2015). While quantifying temperatures using Ti-in-quartz thermobarometry is complicated by uncertainty in activity of TiO_2 (Grujic et al., 2011; Bestmann and Pennacchioni, 2015; Nevitt et al., 2017) and differing calibrations (Huang and Audétat, 2012; Thomas et al., 2015), we find that variations in Ti-in-quartz concentrations in Alpine Fault rocks span a range large enough that these issues can be largely bypassed using independent constraints on maximum and minimum temperatures associated with quartz recrystallization. We have thus generated an extensive Ti-in-quartz data set that facilitates an independent estimate of activity of TiO_2 and places new constraints on the temperatures and pressures at which mylonitisation occurred at deep levels of the Alpine Fault.

2. Background

2.1 Geologic Setting

The Alpine Fault is a major transpressional structure extending ~400 km along the western slopes of New Zealand's Southern Alps, connecting northeastward through the Marlborough fault zone to the Hikurangi subduction zone, and to the southwest to the Puysegur subduction zone (Sutherland et al., 2000). Modern day Alpine Fault systematics began with the onset of a transpressive phase at ~5-8 Ma along the Australia-Pacific plate boundary (e.g. Walcott, 1998; Batt et al., 2004; Cande and Stock, 2004). Mylonites formed during this period have been exhumed in the hanging wall of the Alpine Fault (Norris and Cooper, 2007). The exposed mylonites are developed in the hanging-wall Alpine Schist (referred to below as "the schist"), a complex, predominantly quartzofeldspathic assemblage also containing amphibolite and metachert. Age dating of the Alpine Schist suggests its protolith is an amalgamation of rocks formed at various times from the Carboniferous to Cretaceous (Cooper and Ireland, 2015). Barrovian metamorphic isograds in the non-mylonitic Alpine Schists that are the chief protolith of the Neogene-aged mylonites likely date to the late Cretaceous (e.g. Vry et al., 2004). As the Alpine fault is approached from the east, schist fabrics are overprinted by a classic sequence of fault rocks: protomylonites, mylonites, ultramylonites, and finally cataclasites (Sibson et al., 1979, 1981). Most of the rocks analyzed for this study are from Gaunt Creek, the site of the first drill holes for the 2011 Deep Fault Drilling Project (DFDP, e.g. Boulton et al., 2014). One sample was analyzed from Stony Creek (Fig. 1), 11 km southwest of Gaunt Creek.

Deleted: ure

2.2 Deformation History

Holcombe and Little (2001); Little et al. (2002a; 2002b) and Little (2004) provide detailed microstructural descriptions of the transition from the Alpine Schist to the Alpine Fault mylonite zone. In particular, Little et al. (2002a) recognized four main deformation episodes in the schist (D_1 to D_4). D_4 is Cenozoic deformation related to the evolution of the present dextrally convergent plate boundary (Neogene oblique collision between the Australian and Pacific Plates) and generally reinforces earlier

Mesozoic D_3 fabrics. The present schistosity outside of the Alpine mylonite zone is mostly S_{3-4}. D_4 includes the high-strain mylonitic fabrics within ~1 km of the fault as well as a less conspicuous fabric resulting from distributed transpressional strain in more distal rocks. Neogene deformation incurred a vertical thickening and clockwise rotation (when viewed from the SW) and dextral shearing of the schists. The mylonitic D_4 imprint is only perceptible within 5 km of the Alpine Fault, where it is expressed by shortening (post garnet growth) of at least 50% in a direction perpendicular to the foliation (Holm et al., 1989; Little et al., 2002a). The mylonitic foliation (S_m) that is clearly a product of Alpine Fault-related ductile shearing is subparallel to and strengthens these earlier fabrics, but results from higher strain and thus is aligned nearly parallel to the SE-dipping Alpine Fault.

Mylonitization began at depths of up to 35 km (Grapes, 1995; Vry et al., 2004; Little et al., 2005; Stern et al., 2007; Sutherland et al., 2007). Simple shear strains are γ >150 in the ultramylonites, as high as 120 in the mylonites, and 12-22 in the protomylonites based on thickness of offset, mylonitized pegmatite veins (Norris and Cooper, 2003). Characteristics such as boudinaged quartzose layers parallel to the shear zone, and reorientation of inherited, pre-Neogene lineations indicate that mylonitization involved ductile thinning by a factor >3 (Norris and Cooper, 2003; Gillam et al., 2013; Toy et al., 2013). Kinematic vorticity number (W_k) is estimated to be 0.7-0.85 in the mylonite zone (Little et al., 2016) or higher (Toy et al., 2013). Strain in the mylonite likely had a flattening geometry, but with S_1 exceeding S_2 by ~30 times (Toy et al., 2013). Strain rates were rapid and relatively well constrained at roughly 10^{-12} s^{-1} in the mylonite and ultramylonite zones and around 10^{-13} s^{-1} in the protomylonite zone based on a range of geological and plate tectonic constraints (Norris and Cooper, 2003).

Deleted:

2.3 Previous Temperature Constraints on Alpine Fault Deformation

Thermal models indicate that rapid rates of exhumation in the hanging wall of the central Alpine Fault (~10 mm/yr; Norris and Cooper, 2007) must significantly raise the geothermal gradient in the vicinity of the fault, especially near the surface (e.g. Koons, 1987). Direct measurements of the geothermal gradient in the upper 100's of meters of the crust near our study area are high (95 °C/km, Shi et al., 1996; 63 °C/km, Sutherland et al., 2012; 125 °C/km, Sutherland et al., 2017). Fluid inclusion evidence (e.g. Craw, 1997; Toy et al., 2010), the restriction of most earthquakes to depths <10 km (Leitner. et al., 2001; Boese et al., 2012; Bourguignon et al., 2015), and an observed decrease in temperature gradient near the base of the DFDP-2 borehole (Sutherland et al., 2017) indicate that the geothermal gradient is high near the surface but much lower at deeper levels (Niemeijer et al., 2016). Toy et al. (2008) and Cross et al. (2015) suggested low geothermal gradients in the ductile regime of 10 °C/km and 5 °C/km, respectively.

Thermobarometric data for the Alpine Fault mylonites and Alpine Schists (Cooper, 1980; Grapes and Watanabe, 1992; Grapes, 1995; Vry et al., 2004; Beyssac et al., 2016) indicate that mylonitization began at about 600 °C and 11 kbar. Toy et al. (2008) and Little et al. (2015; 2016) observed crystallographic preferred orientations in quartz that generally form at upper greenschist to amphibolite facies conditions (~500-600 °C). Cross et al. (2015) estimated deformation temperatures of quartz in two samples of at least 450-500 °C based on the c-axis opening angle thermometer (Kruhl, 1996; Law, 2014) and microstructural evidence of subgrain rotation and grain boundary migration recrystallization in quartz (see also Little et al., 2015). The occasional presence of chlorite (generally after biotite) and green, low-Ti biotite indicate some deformation at temperatures as low as greenschist facies in protomylonites and mylonites, with changes in biotite chemistry indicating a decrease in temperature during mylonitic deformation of roughly 340 °C (Toy et al., 2008; Toy et al., 2010). The amphibolite-facies metamorphic assemblage associated with mylonitization is fairly consistent in diverse rock types regardless of distance to the Alpine Fault. Chlorite is not common in

Deleted:

the mylonites or ultramylonites, except in late-stage veins, C' shear bands, and footwall-derived ultramylonites (Toy et al., 2015).

Deleted: either

3. Methods

Samples were analyzed at the California Institute of Technology, with a Cameca 7f Secondary Ion Mass Spectrometer (SIMS) using a $^{16}O^{-}$ primary ion beam. We used a beam current of 10-15 nA, a mass resolving power of 4000, field aperture of 100 mm, and analyzed masses ^{27}Al, ^{30}Si, ^{44}Ca, ^{47}Ti, ^{49}Ti, and in some samples ^{56}Fe. Prior to each analysis, we rastered a 50 x 50 mm area for 60 s. Effective spot size for the analyses was about 10 µm. We used a regression line constrained through the origin (see supplementary materials) to calculate Ti concentrations using 12 analyses of National Institute of Standards (NIST) glasses 610 and 612 (434 ± 15 and 44 ± 5 ppm TiO2 respectively; Jochum et al., 2011). To account for matrix effects between quartz and NIST glass, we applied the correction factor of 0.67 determined by Behr et al. (2010). As a Ti-blank, we used Herkimer 'Diamond', a natural quartz containing 4–5 ppb Ti (Kidder et al., 2013). Analyses of this natural blank suggest an effective detection limit in this study of 78 ± 27 ppb. No blank correction was made. The SIMS analysis routine closely follows that of Kidder et al. (2013), who successfully reproduced known Ti concentrations of two low-Ti quartz standards.

For the subset of samples where Fe was measured (N=170), nearly all of the analyses with Ti concentrations >5 ppm also have high Fe/Si ratios (^{56}Fe/^{30}Si > 0.007, Fig. 2). Analyses with Ti >5 ppm were also not observed to follow any discernable patterns in CL intensity or position in the samples, e.g. nearer cores or rims of grains, while analyses with Ti <5 ppm do show such patterns in many cases. We interpret that all, or nearly all, of the analyses with Ti >5 ppm were contaminated, possibly by trace amounts of Fe-Ti oxide since small grains of Fe-Ti oxide are common in all of the samples. Based on these observations, all analyses with Ti concentrations >5 ppm or ^{56}Fe/^{30}Si > 0.007 (7% of analyses) were removed from the dataset. We were unable to identify any clear criteria to similarly filter the data using Al or Ca concentrations.

Deleted: gure

Cathodoluminescence (CL) images were acquired prior to SIMS analyses on most of the areas where Ti was analyzed using the Zeiss variable-pressure field-emission scanning electron microscope (SEM) at the University of Otago. Images were collected using a variable-pressure secondary electron (VPSE) detector operated at high vacuum, 30 kV accelerating voltage and 7 nA beam current. This detector is sensitive in the range 300–650 nm. Hyperspectral CL maps (MacRae et al., 2013) were acquired in one sample using a JEOL 8500F electron microprobe equipped with an ocean optics QEPro spectrometer tuned to collect from 200-960 nm. The sample for hyperspectral CL mapping was polished with colloidal silica, coated with 15 nm of carbon and analyzed at 20 kV accelerating voltage, 30 nA beam current, dwell time of 40 ms per pixel, and a defocused beam and pixel size of 2 µm. Hyperspectral CL maps were displayed and processed using in-house software, Chimage (Leeman et al., 2012). The hyperspectral maps were fitted at each pixel using a least squares approach with a set of three Gaussian distributions: the Ti^{4+} peak at 470 nm (Leeman et al., 2012), the near infrared peak at 729 nm, and the non-bridging oxygen hole center at 646 nm (Kalceff and Phillips, 1995).

Deleted:

Measurements of grain size, distance between analysis spots and features such as grain boundaries or Ti-bearing phases were made (following SIMS analyses) using a reticle in an optical microscope. Grains were distinguished from subgrains based on the sharpness of grain boundaries under cross-polarized light. Long and short axes of elongate grains were measured, and reported sizes for these grains are diameters of circles with the same area as an ellipse having the measured axes lengths. In order to determine if rutile, a minor constituent in some of the rocks, is present, several hundred to several thousand bright grains in

Deleted: done

Deleted: n

Deleted: following SIMS analyses

backscatter imagery were automatically characterized in each sample using energy-dispersive X-ray spectroscopy (EDS) with the Oxford Instruments particle analysis "Feature" algorithm on the University of Otago SEM.

4. Description of samples

4.1 Schists and Protomylonites

Most of the quartz in the protomylonites and schists has a grain size of 20-200 µm, though grains as large as 2-4 mm are present. Larger grains commonly have patchy undulose extinction, contain subgrains, and are elongated (axial ratios from 1:2 to 1:10) with a distinct shape preferred orientation (SPO). High angle boundaries between the large quartz grains are generally interlobate. In many samples, small (<50 µm) grains are prevalent adjacent to these interlobate boundaries. Feldspars form porphyroclasts and show little evidence of crystal plasticity--only weak undulose extinction and in some cases deformation twins. Since both subgrains and, more commonly, relatively large grains with interlobate high-angle grain boundaries are observed, the observed quartz microstructures resemble those of the regime 2/3 transition to lower regime 3 described by Hirth and Tullis (1992) in experimentally deformed quartzites. C' shear bands, some containing a retrograde chlorite-bearing assemblage, are pervasively developed in the protomylonites (Gillam et al., 2013). These contain recrystallized quartz grains as small as 10-20 µm.

4.2 Mylonites and Ultramylonites

Towards the Alpine Fault the mineral phases in the quartzofeldspathic mylonites and ultramylonites become more mixed and grain size (all grains, i.e. recrystallized plus inherited grains) decreases. S-C and C' fabrics are abundant. Minor chlorite is present in some rocks but is less abundant than in the protomylonites. Within a few hundred meters of the Alpine Fault, phase mixing is pronounced, particularly in ultramylonite layers, and domains of pure quartz are restricted to rare foliation-parallel veins and metachert layers. Quartz aggregates generally consist of slightly elongate (axial ratios mostly >2:1) grains of size 40 - 100 µm. Except in the metacherts and deformed pure quartz veins, large quartz grains with undulose extinction are much rarer in the ultramylonites and mylonites than in the protomylonites. The maximum typical long axis of quartz grains in the mylonites is around 1 mm and decreases in size towards the fault. The larger quartz grains in the mylonites are bounded by interlobate high-angle boundaries, with only weak undulose extinction and occasional aggregates of subgrains. In mylonitic metachert samples, secondary phases are often encased in quartz, which often forms elongate, ribbon-like foliation-parallel grains bounded by micas. These quartz grains display castellate microstructures, pinning and other indicators of high-temperature grain boundary migration (Jessel, 1987; Little et al., 2015). Within ~100 m of the fault, rare concentrations of quartz are often strongly recrystallized with a recrystallized grain size on the order of 10-20 µm. In these samples, ribbon grains are common and often filled with 10-20 µm subgrains (Fig. 3) suggesting subgrain rotation recrystallization was a dominant process (Hirth and Tullis, 1992; Stipp et al., 2002).

5. Cathodoluminescence

Cathodoluminescence (CL) intensity generally correlates with Ti concentration such that bright CL corresponds with high Ti concentrations (Wark and Spear, 2005), and several studies have utilized panchromatic CL signal as a proxy for Ti concentrations (Spear et al., 2012; Bestmann and Pennacchioni, 2015; Nevitt et al., 2017). Typical CL images of the Alpine Fault mylonites and protomylonites show a homogeneous illumination (e.g. Fig. 4a), generally with a thin dark rim around the edges of grains (note that this relationship is reversed in the hyperspectral CL images in Fig. 4a and 4b that show brighter rims). Rare

Deleted: ure

Deleted: .

samples contain grains with gradients in CL, typically large grains with higher CL that diminishes gradually towards grain edges. In these cases, Ti concentrations are generally correlated with panchromatic CL, however several exceptions to this pattern were noted. The typical association of recrystallized grains with darker-CL and low Ti (e.g. Kidder et al., 2013) was rarely observed in the mylonites and protomylonites, but is common in the ultramylonites. The sample analyzed using hyperspectral CL has a homogeneous Ti concentration, so the typical association of blue light intensity and higher Ti (Wark and Spear, 2005) was not observed, and instead variation in the blue wavelength signal is seen to be a function of grain orientation (Fig. 4). We note that both these anomalous results and those of Kidder et al. (2013), who found a brighter blue CL signal in recrystallized areas, were observed in quartz with Ti concentrations much lower than typically measured (e.g. Wark and Spear, 2005).

6. Ti-in-quartz concentrations: observations

6.1 General observations

The bulk composition of Alpine Schist samples does not appear to be a significant factor controlling the Ti concentration in their quartz grains. Neighboring felsic and mafic schists have ranges of Ti concentration that broadly overlap, although a few amphibolite and metachert samples have up to ~1 ppm higher Ti concentrations than nearby quartzofeldspathic schists (Fig. 5). The presence of chlorite and rutile in samples (Table 1) is also not systematically associated with higher or lower Ti concentrations. In samples containing rutile, it's abundance relative to other oxides varies from about 2% to 97%, but these values are not correlated with average Ti-in-quartz concentrations of the samples.

The range of Ti values increases with decreasing grain size (Fig. 6)(c.f. Kidder et al., 2013). Grains larger than ~200 µm in the two creeks have indistinguishable Ti concentrations, but smaller grains in two samples from Stony Creek (including one from Cross et al., 2015) have lower Ti values than observed in Gaunt Creek (Fig. 6). Fig. 7 plots Ti concentration versus distance to grain boundaries (Fig. 7a) and distance to any dark mineral likely to contain Ti as a major component such as biotite, hornblende, ilmenite, magnetite or rutile (Fig. 7b). Ti concentrations have values of 2-4 ppm Ti for nearly all analyses further than 50 µm from grain edges, whereas lower values gradually become more common closer to grain boundaries. The low frequency of Ti values <1 ppm Ti at distances from grain boundaries <5 µm may be a function of minor contamination along grain boundaries (Fig. 7a). The potential effect of proximity to minerals containing non-trace amounts of Ti (mainly biotite and Fe-Ti oxide) appears to be minimal (Fig. 7b). The lowest Ti quartz grains (Ti <0.8 ppm) were only found >50 µm from Ti-bearing phases (Fig. 7b). In one metachert sample (77913), a transect away from a large rutile grain showed no variation in Ti with distance from the grain.

6.2 Observations: Schists, Protomylonites, and Mylonites

Because high temperature dynamic recrystallization can involve resetting of Ti contents as grain boundaries sweep through quartz (e.g. Grujic et al., 2011), it is non-trivial to ascertain whether the limited range of 2-4 ppm Ti in grains coarser than ~250 µm (Fig. 6) indicates initial Ti concentrations prior to Alpine Fault motion, or whether they were reset by prolonged high temperature deformation. Most quartz-rich layers have relatively homogeneous Ti concentrations (Fig. 4) as commonly observed in samples that experienced protracted high-temperature metamorphism (e.g. Spear and Wark, 2009).

In the Gaunt Creek mylonites and protomylonites, recrystallized grains of all sizes generally have Ti contents that are also in the same 2-4 ppm range as the coarser grains, although some moderate-sized (20-200 µm) grains with Ti concentrations in the range 1-2 ppm are also present (Fig. 8). In individual samples, Ti concentrations are often homogenous, varying with no systematic spatial pattern between about 2 and 4 ppm (e.g. Fig. 4). Some samples do contain local, minor-but-systematic variations in Ti within this range of values, however no over-arching pattern was observed. For example, in sample 77886, Ti increases from ~2.5 to 3.5 ppm where a quartz layer is pinched, recrystallized, and finer-grained adjacent to a garnet porphyroclast. Quartz in a similar microstructural setting was not associated with a consistent change in Ti in the Alpine Fault rocks studied by Cross et. al. (2015). Two metachert samples (77920 and 77923) contain 400 µm thick quartz layers with low-Ti central areas in the range 1-2.5 ppm Ti that increase to ~3 ppm at their edges. A similar pattern is observed in protomylonite sample 77982, and could be interpreted as indicating lower initial Ti values than 2-4 ppm for these rocks. Several large quartz grains in sample 77982 also have bright-CL cores suggesting different "initial" Ti between the metachert and quartzofeldspathic portions of the sample. At a larger scale, there is a gradual decrease in average Ti concentrations of 3-4 ppm at structural distances of 500 m from the Alpine Fault to values closer to 2-3 ppm at 1100 m (Fig. 9). This pattern is particularly evident in coarse grains (Fig. 9 inset).

Two samples, a protomylonite and a mylonite (77875 and 77925), contain late, chlorite-bearing quartz veins that cut foliation. Quartz in both veins shows evidence of minor dynamic recrystallization and has Ti concentrations of 2-4 ppm. Given the high shear strains experienced by the Alpine Fault mylonites (Norris and Cooper, 2003), these late-stage veins formed during the last few percent of penetrative mylonitic strain. The presence of chlorite in these veins constrains their emplacement temperatures and therefore the cessation of mylonitization to within the chlorite stability field, a wide temperature range from 360 °C to 500 °C in Alpine Fault rocks (Vry et al., 2007; Beyssac et al., 2016).

Fine recrystallized quartz in two of three C' type shear bands shows evidence of lower Ti-in-quartz concentrations than surrounding quartz. A C' shear band from a Stony Creek sample (same as sample ST_12 in Little et al., 2016) shows a marked decrease in Ti concentrations within the shear band (Fig. 10). In Gaunt Creek, quartz in one C' band from near the mylonite-protomylonite boundary (77886) shows a lower Ti content (~2.25 ppm) than quartz in the foliation that is cross-cut (~3.5 ppm Ti). A shear band in protomylonite sample 5.2.1.13, however, shows little to no decrease in Ti in a (chlorite-absent) C' band.

6.3 Observations: Ultramylonites

The population of quartz grains in ultramylonites of size >30 µm generally have indistinguishable, or slightly lower, Ti concentration when compared to rocks further from the fault (Fig. 8). Finer grains, however, are distinctly shifted to lower values (1-2.5 ppm vs. values of 2-4 ppm in the mylonites and protomylonites). This trend is associated with a decrease in average quartz grain size and a deviation from the higher Ti concentrations in adjacent coarser grains (Fig. 9). This pattern is evident in individual transects from coarser-grained areas to finer-recrystallized areas with decreased Ti concentrations of 1-2 ppm in both ultramylonite samples as well as the closest mylonite sample (77911) to the Fault (e.g. Fig. 3).

7. Discussion

7.1 Evolution of Ti concentrations

7.1.1 Initial Ti-in-quartz concentrations were 2-4 ppm

Coarse polygonal quartz grains in non-mylonitic schist outside the present study area are inferred to have formed in the Mesozoic during an extended, non-orogenic period when the rocks resided at high temperature in the middle to lower crust (Little, 2004), i.e. prior to their Neogene exhumation resulting from shearing on the Alpine Fault. The roughly 30 coarse grains analyzed (>250 µm) from schist and mylonite samples in our study contain a restricted range of Ti concentrations of 2-4 ppm

Deleted: Figure

Deleted: Figure

Deleted: s

Deleted: Figure

Deleted: Figure

Deleted: Figure

Deleted: Figure

Deleted: s

Deleted: Figure

(Fig. 6), and given their large size (some >1 mm), we also infer these to be Mesozoic grains. The characteristic diffusion timescale (e.g. Spear, 1995) for 250 µm grains using the experimental data of Cherniak et al. (2007) at a peak Alpine Fault mylonitization temperature of ~550 °C (Toy et al., 2010; Cross et al., 2015) is 1.5 Ga, seemingly barring the possibility that these grains were reset by diffusional processes during mylonitization lasting a few million years in the Neogene. We interpret that the 2-4 ppm Ti-in-quartz concentrations in large grains were stabilized during Mesozoic metamorphism, prior to Neogene Alpine Fault related deformation.

The significance of the apparent trend in Ti concentrations of the largest grains in the Gaunt Creek section towards higher Ti concentrations at deeper structural levels (Fig. 9 inset) is unclear. If the variation in initial Ti concentration were purely the result of differences in initial depth along a vertical column of rock, the position of the isopleths in Fig. 11 would indicate a stretch perpendicular to foliation of 1/7, more than twice the foliation-perpendicular component estimated in previous studies (Holm et al., 1989; Holcombe and Little, 2001; Toy et al., 2013). It is worth noting, however, that because of the extreme simple shear strains experienced by the Alpine Fault mylonites, the various hanging wall rocks sampled for this study and presently separated by distances <1 km, were originally separated by >100 km (Norris and Cooper, 2003). Given these large offsets, it is possible that the large apparent shortening was a function of pre-Alpine Fault regional variations in geothermal gradient (i.e. a regional variability in initial Ti concentration at a given depth), and/or shallowing of the hypothesized deep, semi-horizontal continuation of the Alpine Fault towards the east (Batt and Braun, 1997; Little et al., 2002a; Cox and Sutherland, 2007).

7.1.2 Protomylonite & Mylonite Deformation occurred along a Geothermal Gradient of 5 °C/km

Two observations support a hypothesis that the pre-Alpine Fault 2-4 ppm range of Ti-in-quartz concentrations was stable for nearly the entire period of protomylonite and mylonite deformation. First, slightly-deformed chlorite-bearing quartz veins that cross-cut foliation also have Ti concentrations of 2-4 ppm. Second, small quartz grains generated in the mylonites and protomylonites during Alpine Fault deformation contain similar concentrations of Ti as coarser grains (e.g. Fig. 4, 8). This is atypical behavior, since increasingly finer grains formed during exhumation generally show systematic changes in Ti concentration (e.g. Kohn and Northrup, 2009; Behr and Platt, 2011; Kidder et al., 2013; the Alpine Fault ultramylonites described in this manuscript). We suggest that, as commonly observed, gradually increasing stresses due to strengthening during cooling also led to an increasingly fine-grained overprint during exhumation of the Alpine Fault mylonites. The unvarying Ti-in-quartz concentrations in the Alpine Fault can be explained then if the exhumation path happened to coincide with a contour of constant-Ti concentration in pressure-temperature space (an "isopleth," Fig. 11). The isopleths plotted in Fig. 11 are based on the experimental results of Thomas et al. (2010) and correspond to a slope of 5 °C/km, a plausible value that is identical to the deep geothermal gradient proposed by Cross et al. (2015) based on different criteria. Thus, despite a significant decrease in temperature, Ti levels of 2-4 ppm remained stable during the bulk of Alpine Fault mylonitization.

7.1.3 Ultramylonite Deformation involved a decrease in stable Ti levels to 1-2 ppm

In the ultramylonites, Ti-in-quartz concentrations in grains coarser than 50 µm are generally indistinguishable from those in protomylonites and mylonites, however lower Ti concentrations (1-2 ppm) are much more common in fine recrystallized grains in the ultramylonites (Fig. 8). We interpret the clustering of Ti-in-quartz values in the range 1-2 ppm in the recrystallized areas of several ultramylonite samples as indicating the equilibrium concentration associated with the latest phase of quartz recrystallization near the Alpine Fault. Note that the spread of Ti-in-quartz concentrations in fine grains generated during late recrystallization (Fig. 8, 9, 10) suggests that dynamic recrystallization was not 100% effective in shifting Ti concentrations to

Deleted: Figure
Deleted: byr.
Deleted: Figure
Deleted: Figure
Deleted: Figures
Deleted: Figure
Deleted: figure
Deleted: Figures
Deleted: Figures

equilibrium values, as observed elsewhere (e.g. Haertle et al., 2013; Kidder et al., 2013; Bestmann and Pennacchioni, 2015; Nevitt et al., 2017).

7.1.4 Latest Deformation Involving Quartz Recrystallization Occurred Off-Fault

The lowest Ti concentrations measured in this study (0.5-0.8 ppm) come from within a chlorite-bearing C' shear band in a protomylonite sample from Stony Creek (Fig. 10). C' shear bands are abundant in Alpine Fault protomylonites (Little et al., 2016) and elsewhere, and are widely understood to be late deformation features (e.g. Toy et al., 2012) accommodating minor amounts of strain relative to the total mylonitic deformation (Gillam et al., 2013). The low Ti-in-quartz concentrations in this shear band, as well as the decreased Ti concentrations in one of two Gaunt Creek shear bands analyzed, are consistent with partial resetting during a late stage of low-temperature deformation.

The Stony Creek mylonite sample analyzed by Cross et al. (2015) contains very low Ti concentrations (0.2-0.4 ppm) in relatively large grains (up to 130 µm) not microstructurally associated with any obvious late deformation phase. Thus, at face value, the very last quartz grains to recrystallize were not in localized C' zones, but were instead fairly moderate-sized quartz grains not associated with shear bands or another type of microstructure indicative of late, low-temperature deformation. Anomalously low Ti concentrations were also observed locally in Gaunt Creek, but the Ti values are not as low (0.5-1 ppm; Fig. 6). It is unclear if these observations are influenced by some difference between Stony and Gaunt creeks, but it is noteworthy that the two samples from Stony Creek have the lowest Ti-in-quartz measurements observed. Possibly deformation in Stony Creek continued at lower temperatures than in Gaunt Creek (11 km to the NE) or there was a difference in the geothermal gradient between the two creeks. The two creeks show at least one compositional difference (more metacherts in Stony creek), so it is also possible that some systematic compositional differences might have reduced activity of TiO_2 in Stony Creek. If differences in bulk composition between the two creeks were the cause, however, we would not expect coarse grains in the two creeks to have indistinguishable Ti concentrations (Fig. 6), nor would we expect an absence of a compositional effect locally in Gaunt Creek samples (Fig. 5).

In any case, the presence of Ti concentrations <0.8 ppm along C' shear bands and elsewhere in the protomylonite zone, and absence of such values closer to the fault suggests that the latest phase of deformation involving dynamic recrystallization of quartz did not take place in the ultramylonites as might be expected based on general models of shear zones involving increased localization at shallower depths (e.g. Sibson, 1977). Instead, the latest phase of deformation involving quartz recrystallization occurred in a broad region of protomylonites and mylonites outside the fault core. Toy (2007) reached the same conclusion based on observation of a more retrograde mineral assemblage associated with C' shear bands. An explanation for this may be illustrated in strength-depth diagrams plotting flow laws at different strain rates (e.g. Kidder et al., 2012): near the brittle-ductile transition, deformation at slow strain rates will be in the plastic regime, while at the same pressure-temperature conditions, faster strain rates can be accommodated with less resistance by brittle mechanisms. We suggest that near the BDT, as strain rates increased in the narrow (<10 m-wide) cataclastic zone, deformation away from this localized zone remained slow enough to favor some dislocation creep. Put differently, the brittle-plastic transition extended to deeper levels near the fault than away from it, as predicted in numerical models of the Alpine Fault by Ellis and Stöckhert (2004).

7.2 Activity of TiO_2

The activity of TiO_2 (a_{TiO2}) has proven to be a major source of uncertainty in previous studies (e.g. Grujic et al., 2011; Nevitt et al., 2017), apparently varying by nearly an order of magnitude in previous studies of quartzofeldspathic rocks from values as

Deleted: Figure

Deleted: Figure

Deleted: Figure

Deleted: Figure

high as 1.0 (Kidder et al., 2013) to 0.2 (Grujic et al., 2011). The lack of knowledge of a_{TiO2} and the factors that control it complicates quantitative estimation of temperature using the TitaniQ thermobarometer. Establishing Ti activities in natural samples is also hindered by competing calibrations of TitaniQ (Thomas et al., 2010; Huang and Audétat, 2012; Thomas et al., 2015). While we employ the calibration of Thomas et al**.** (2010; 2015), we note that using the Huang and Audetat (2012) calibration would not substantially change our results (apart from the estimated a_{TiO2}) because the two calibrations have similar slopes in pressure-temperature space at pressures >2 kbar (see Figure 6 of Kidder et al., 2013).

Despite these uncertainties, sufficient independent information is available for Alpine Fault rocks to constrain their a_{TiO2} to a very low value of 0.1 (using the Thomas et al., 2010 calibration). This value is estimated assuming that the lowest observed Alpine Fault Ti-in-quartz concentrations of ~0.2 ppm represent deformation at the low-temperature limit for dynamic recrystallization of quartz of 300 °C (Dresen et al., 1997; Dunlap et al., 1997; Stöckhert et al., 1999; van Daalen et al., 1999; Stipp et al., 2002), and using the relatively steep (>50 °C/km) upper crustal geothermal gradient indicated by fluid inclusions (e.g. Toy et al., 2010)(Fig. 11) and borehole data in the vicinity of the study area (Sutherland et al., 2012; Sutherland et al., 2017). The lower limit of 0.2 ppm Ti has also been observed in Alpine Fault rocks to the south near the Haast River (Kidder et al., 2016a). Using a higher a_{TiO2} would require that recrystallization of quartz took place at unrealistically low temperatures (Fig. 11). An activity of TiO_2 of 0.1 also places the estimated initial Ti concentration of ~3 ppm at a temperature of 600 °C near the base of the crust, consistent with the thermobarometric constraints from Vry et al. (2004) that mylonitization began at around 600 °C and 11 kbar. A similar analysis using the Ti-in-quartz calibration of Huang and Audetat (2012) would involve an activity of TiO_2 in the range 0.5-0.8 (e.g. as adopted by Cross et al., 2015).

While it is convenient to assign a single value of a_{TiO2} to a suite of rocks such as our sample set—and the overall consistency of Ti-in-quartz concentrations in different lithologies generally supports this (Fig. 5)—sample- or micro-scale variations in a_{TiO2} due to local differences in bulk or fluid composition may exist. Additionally, activity of TiO_2 could also vary with temperature (Ashley and Law, 2015). An absence of Ti values less than ~1 ppm at distances <50 µm from phases containing stoichiometric quantities of Ti (Fig. 7B) hints at both types of a_{TiO2} variation. The absence of Ti values <1 ppm could be explained if a_{TiO2} was higher than 0.1 in the vicinity of high-Ti minerals during the latest phase of quartz recrystallization. A change in a_{TiO2} to a value of 0.5 in the immediate vicinity (<50 µm) of Ti-bearing phases at temperatures of 300 °C would stabilize Ti concentrations at 1 ppm and explain the local absence of lower Ti measurements. The extent of recrystallization at these conditions was minor, as suggested by the low frequency of such analyses (Fig. 7) and their location only within 30 µm of grain boundaries (Fig. 7a).

7.3 Geothermal Gradient of the Alpine Fault

Considering that long term average strain rates are well-established in the Alpine Fault mylonites at ~10^-12 s^-1 (Norris and Cooper, 2003), we can place a rough estimate on the minimum temperature of mylonite deformation using a piezometer and flow law. The average recrystallized grain size in the Alpine Fault mylonites is in the range of 40-70 µm (Toy, 2007; Lindroos, 2013; Little et al., 2015), corresponding with stresses of 31-44 MPa (Cross et al., 2015) and a temperature of 430-480 °C using the quartz flow law from Kidder et al. (2016b). The intersection of the 3 ppm isotherm and this temperature range occurs at depths of 0-8 km (Fig. 11), thereby requiring an order of magnitude change in slope from about 5 °C/km to at least 60 °C/km at depths of 8 km or less. We adopt the values (60 °C/km above 8 km) that minimize the magnitude of the kink, although shallower kinks and larger upper crustal geothermal gradients would also fit the data presented here. This upper crustal geothermal gradient falls close to the geothermal gradient of 63 ± 2 °C/km measured in the upper 140 meters of the DFDP- 1B borehole site at Gaunt

Deleted: figure

Deleted:

Deleted: figure

Deleted: Figure

Deleted: Figure

Deleted: Figure

Deleted: Figure

Deleted: Figure

Creek (Sutherland et al., 2012), although it is clear that there is considerable local variation in the upper crustal geothermal gradient likely due to fluid circulation associated with topography (Sutherland et al., 2017). The Alpine Fault geothermal gradient predicted here is very similar to that presented by Cross et al. (2015)—differing only in the slightly shallower position of the kink at 480 °C in this study (vs. 495 °C), and the correspondingly larger upper-crustal geothermal gradient in our analysis (Fig. 11). The general shape of a large upper crustal geothermal gradient and low geothermal gradient at deeper levels was also predicted by early two-dimensional numerical models of Alpine Fault exhumation (Koons, 1987; Figure 11), wherein rapid uplift leads to significant heat advection towards the surface followed by heat loss by conduction in a region of condensed near-surface isotherms. The position of the kink in this study also corresponds roughly to the maximum depth of earthquakes near the study area (Boese et al., 2012; Leitner. et al., 2001), suggesting that the onset of rapid cooling reduces temperatures to conditions where brittle processes dominate, and/or that fracturing associated with seismicity accentuates cooling by the infiltration of meteoric fluids to deep levels (Menzies et al., 2014).

Despite the similarities between the geothermal gradient presented here and that of Cross et al. (2015), there are significant differences in our microstructural interpretations stemming from the much larger dataset and variety of rock types examined in this study. Cross et al. (2015) interpreted that the restricted range of Ti concentrations in their two protomylonite samples were established rapidly, in a narrow window of temperatures (450-500 °C) above the kink in the geothermal gradient. Alternatively, we attribute the restricted range of Ti concentrations to deformation along a constant Ti isopleth below the kink—a scenario not considered by Cross et al. (2015). In their interpretation, the microstructures are essentially a snapshot of a rapidly changing grain configuration, whereas we hypothesize that larger grains were preserved from before and throughout Alpine Fault deformation and that these grains record a history of equilibrium Ti concentrations that happens to have varied little over time. We propose the new hypothesis because of our identification of two phases of Ti-in-quartz behavior (e.g. Fig. 12). In the earlier phase (phase 1), coarse grains with a homogenous Ti concentration were established (Fig. 6, 8). The development of finer grains during late phase 1 deformation was not associated with significant systematic changes in Ti concentration (e.g. Fig. 4, 8). Alternatively, phase 2, associated with ultramylonites (Fig. 3, 8) and C' fabrics (Fig. 10), is marked by decreased Ti-in-quartz concentrations in recrystallized grains as the exhumation path ceased following a constant-Ti isopleth and began crossing Ti isopleths (Fig. 11).

8. Conclusions

The vast majority of the mylonitic deformation of the Alpine Fault occurred while rocks were exhumed from depths of around 35 km to around 8 km while cooling by only 120 °C (from 600 °C to 480 °C) along a geothermal gradient of 5 °C/km. Assuming a constant exhumation rate, cooling rates increased at a depth of 8 km by an order of magnitude as the geothermal gradient increased to about 60 °C/km. The transition at 8 km corresponds roughly to the position of the knee in the geothermal gradient predicted by simple two dimensional models of exhumed faults (Koons, 1987), as well as the lower limit of seismicity (Leitner. et al., 2001; Boese et al., 2012) and the formation of ultramylonites in the fault core. Deformation at temperatures <400 °C was dominated by brittle processes such as cataclasis on and near (within ~30 m of) the Alpine Fault, and, until a temperature of 300 °C was reached, minor ductile deformation in protomylonites away from the fault. Despite major uncertainties in activity of TiO_2, Ti-in-quartz data can provide valuable quantitative constraints on deformation temperature and geothermal gradients.

Acknowledgments

We are grateful for helpful conversations with Andrew Cross. Yunbin Guan provided critical assistance with the SIMS, and Brent Pooley prepared thin sections. Funding for the project was supplied by NSF grants IRFP-1064805 and EAR-1524602.

References

Ashley, K. T. and Law, R. D.: Modeling prograde TiO2 activity and its signicance for Ti-in-quartz thermobarometry of pelitic metamorphic rocks, Contributions to Mineralogy and Petrology, 169, doi:10.1007/s00410-015-1118-7, 2015.

Batt, G. E., Baldwin, S. L., Cottam, M., Fitzgerald, P. G., and Brandon, M. T.: Cenozoic plate boundary evolution in the South Island of New Zealand: new thermochronological constraints, Tectonics, 23, TC4001, 2004.

Batt, G. E. and Braun, J.: On the thermomechanical evolution of compressional orogens, Geophysical Journal International, 128, 364-382, 1997.

Batt, G. E. and Braun, J.: The tectonic evolution of the Southern Alps, New Zealand: insights from fully thermally coupled dynamical modelling, Geophysical Journal International, 136, 403-420, 1999.

Batt, G. E., Braun, J., Kohn, B. P., and McDougall, I.: Thermochronological analysis of the dynamics of the Southern Alps, New Zealand, Geological Society of America Bulletin, 112, 250-266, 2000.

Behr, W. M. and Platt, J. P.: A naturally constrained stress profile through the middle crust in an extensional terrane, Earth and Planetary Science Letters, 303, 181-192, doi:10.1016/J.Epsl.2010.11.044, 2011.

Behr, W. M., Thomas, J., and Hervig, R.: Calibrating Ti concentrations in quartz on the SIMS using NIST silicate glasses with applications to the TitaniQ geothermobarometer, American Mineralogist, 96, 1100-1106, doi:10.2138/am.2011.3702, 2010.

Bestmann, M. and Pennacchioni, G.: Ti distribution in quartz across a heterogeneous shear zone within a granodiorite: The effect of deformation mechanism and strain on Ti resetting, Lithos, 227, 37-56, doi:10.1016/j.lithos.2015.03.009, 2015.

Beyssac, O., Cox, S. C., Vry, J., and Herman, F.: Peak metamorphic temperature and thermal history of the Southern Alps (New Zealand), Tectonophysics, 229-249, doi:10.1016/j.tecto.2015.12.024, 2016.

Boese, C. M., Townend, J., Smith, E., and Stern, T.: Microseismicity and stress in the vicinity of the Alpine Fault, central Southern Alps, New Zealand, Journal of Geophysical Research, 117, doi:10.1029/2011JB008460, 2012.

Boulton, C., Moore, D., Lockner, D. A., Toy, V. G., Townend, J., and Sutherland, R.: Frictional properties of exhumed fault gouges in DFDP-1 cores, Alpine Fault, New Zealand, Geophysical Research Letters, 41, doi:10.1002/2013GL058236, 2014.

Bourguignon, S., Bannister, S., Henderson, C. M., Townend, J., and Zhang, H.: Structural heterogeneity of the midcrust adjacent to the central Alpine Fault, New Zealand: Inferences from seismic tomography and seismicity between Harihari and Ross Geochemistry Geophysics Geosystems, 16, 1017-1043, doi:10.1002/2014GC005702, 2015.

Cande and Stock, J.: Pacific-Antarctic-Australia motion and the formation of the Macquarie Plate, Geophysical Journal International, 157, 399-414, 2004.

Chamberlain, C. J., Shelly, D. R., Townend, J., and Stern, T. A.: Low-frequency earthquakes reveal punctuated slow slip on the deep extent of the Alpine Fault, New Zealand, Geochemistry Geophysics Geosystems, 15, doi:10.1002/2014GC005436, 2014.

Cherniak, D. J., Watson, E. B., and Wark, D. A.: Ti diffusion in quartz, Chem Geol, 236, 65-74, doi:10.1016/J.Chemgeo.2006.09.001, 2007.

Cooper, A. F.: Retrograde alteration of chromian kyanite in metachert and amphibolite whiteschist from the Southern Alps, New Zealand, with implications for uplift on the Alpine Fault, Contributions to Mineralogy and Petrology, 75, 153-164, doi:10.1007/BF00389775, 1980.

Cooper, A. F. and Ireland, T. R.: The Pounamu terrane, a new Cretaceous exotic terrane within the Alpine Schist, New Zealand; tectonically emplaced, deformed and metamor- phosed during collision of the LIP Hikurangi Plateau with Zealandia, Gondwana Research 27, 1255-1269, doi:10.1016/j.gr.2013.11.011 2015.

Cox, S. and Sutherland, R.: Regional Geological Framework of South Island, New Zealand, and its Signi cance for Understanding the Active Plate Boundary. In: A Continental Plate Boundary: Tectonics at South Island, New Zealand Geophysical Monograph Series 175, 2007.

Craw, D.: Fluid inclusion evidence for geothermal structure beneath the Southern Alps, New Zealand, New Zealand Journal of Geology and Geophysics, 40, 43-52, doi:10.1080/00288306.1997.9514739, 1997.

Cross, A. J., Kidder, S., and Prior, D.: Using quartz sheared around garnet porphyroclasts to evaluate microstructural evolution in nature, Journal of Structural Geology, 75, 17-31, doi:10.1016/j.jsg.2015.02.012, 2015.

Dresen, G., Duyster, J., Stöckhert, B., Wirth, R., and Zulauf, G.: Quartz dislocation microstructure between 7000 m and 9100 m depth from the Continental Deep Drilling Program KTB, Journal of Geophysical Research, 102, 18,443-418,452, 1997.

Dunlap, W., Hirth, G., and Teyssier, C.: Thermomechanical evolution of a ductile duplex, Tectonics, 16, 983-1000, 1997.

Ellis, S. and Stöckhert, B.: Elevated stresses and creep rates beneath the brittle-ductile transition caused by seismic faulting in the upper crust, Journal of Geophysical Research, 109, doi:10.1029/2003JB002744, 2004.

Gillam, B. G., Little, T. A., Smith, E., and Toy, V. G.: Extensional shear band development on the outer margin of the Alpine mylonite zone, Tatare Stream, Southern Alps, New Zealand, Journal of Structural Geology, 54, 1-20, doi:10.1016/j.jsg.2013.06.010, 2013.

Grapes, R. and Watanabe, T.: Metamorphism and uplift of Alpine schist in the Franz Josef-Fox Glacier area of the Southern Alps, New Zealand, metamophic Geology, 10, 171-180, 1992.

Grapes, R. H.: Uplift and exhumation of Alpine Schist, Southern Alps, New Zealand: thermobarometric constraints, New Zealand Journal of Geology and Geophysics, 38, 525-533, 1995.

Grujic, D., Stipp, M., and Wooden, J. L.: Thermometry of quartz mylonites: Importance of dynamic recrystallization on Ti-in-quartz reequilibration, Geochemistry Geophysics Geosystems, 12, Q06012, doi:10.1029/2010GC003368, 2011.

Haertle, M., Herwegh, M., and Pettke, T.: Titanium-in-quartz thermometry on synkinematic quartz veins in a retrograde crustal-scale normal fault zone, Tectonophysics, 608, 468-481, doi:10.1016/j.tecto.2013.08.042, 2013.

Herman, F., Braun, J., and Dunlap, W. J.: Tectonomorphic scenarios in the Southern Alps of New Zealand, J Geophys Res-Sol Ea, 112, -, doi:10.1029/2004jb003472, 2007.

Hirth, G. and Tullis, J.: Dislocation creep regimes in quartz aggregates, Journal of Structural Geology, 14, 145-159, 1992.

Holcombe, R. J. and Little, T. A.: A sensitive vorticity gauge using rotated porphyroblasts, and its application to rocks adjacent to the Alpine Fault, New Zealand, Journal of Structural Geology, 23, 979-989, 2001.

Holm, D. K., Norris, R. J., and Craw, D.: Brittle and ductile deformation in a zone of rapid uplift: Central Southern Alps, New Zealand, Tectonics, 8, 153-168, 1989.

Huang, R. and Audétat, A.: The titanium-in-quartz (TitaniQ) thermobarometer: A critical examination and re-calibration, Geochim Cosmochim Ac, 84, 75-89, doi:10.1016/j.gca.2012.01.009, 2012.

Jessel, M. W.: Grain-boundary migration microstructures in a naturally deformed quartzite, Journal of Structural Geology, 9, 1007-1014, doi:10.1016/0191-8141(87)90008-3, 1987.

Jochum, K. P., Weis, U., Stoll, B., Kuzmin, D., Yang, Q., Raczek, I., Jacob, D. E., Stracke, A., Birbaum, K., Frick, D. A., Günther, D., and Enzweiler, J.: Determination of Reference Values for NIST SRM 610--617 Glasses Following ISO Guidelines, Geostandards and Geoanalytical Research, 35, 397-429, doi:10.1111/j.1751-908X.2011.00120.x, 2011.

Kalceff, M. A. S. and Phillips, M. R.: Cathodoluminescence microcharacterisation of the defect structure of quartz, Physical Review B, 52, 3122-3144, 1995.

Kidder, S., Toy, V., Prior, D., and Little, T.: The Effect of Recrystallization on Titanium Concentrations in Quartz, an Example from New Zealand's Alpine Fault, American Geophysical Union Annual Meeting, 2016.

Kidder, S. B., Avouac, J. P., and Chan, Y. C.: Application of titanium-in-quartz thermobarometry to greenschist facies veins and recrystallized quartzites in the Hsüehshan range, Taiwan, Solid Earth, 4, 1-21, doi:10.5194/se-4-1-2013, 2013.

Kidder, S. B., Avouac, J. P., and Chan, Y. C.: Constraints from rocks in the Taiwan orogen on crustal stress levels and rheology, Journal of Geophysical Research, 117, doi:10.1029/2012JB009303, 2012.

Kidder, S. B., Hirth, G., Avouac, J. P., and Behr, W. M.: The influence of stress history on the grain size and microstructure of experimentally deformed quartzite, Journal of Structural Geology, 83, 194-206, doi:10.1016/j.jsg.2015.12.004, 2016b.

Kohlstedt, D. L., Evans, B., and Mackwell, S. J.: Strength of the lithosphere–constraints imposed by laboratory experiments, J Geophys Res-Sol Ea, 100, 17587-17602, 1995.

Kohn, M. J. and Northrup, C. J.: Taking mylonites' temperatures, Geology, 37, 47-50, doi:10.1130/G25081A.1, 2009.

Koons, P. O.: Some thermal and mechanical consequences of rapid uplift: an example from the Southern Alps, New Zealand, Earth and Planetary Science Letters, 86, 307-319, 1987.

Kruhl, J. H.: Prism- and basal-plane parallel subgrain boundaries in quartz: a microstructural geothermobarometer, Journal of Metamorphic Geology, 14, 581-589, 1996.

Law, R. D.: Deformation thermometry based on quartz c-axis fabrics and recrystallization microstructures: A review., Journal of Structural Geology, 66, 129-161, doi:10.116/j.jsg.2014.05.023 2014.

Leeman, W. P., MacRae, C. M., Wilson, N. C., Torpy, A., Lee, C.-T. A., Student, J. J., Thomas, J. B., and E.P., V.: A Study of Cathodoluminescence and Trace Element Compositional Zoning in Natural Quartz from Volcanic Rocks: Mapping Titanium Content in Quartz., Microscopy and Microanalysis, 18, 1322-1341, 2012.

Leitner., B., Eberhart-Phillips, D., Anderson, H., and Nabelek, J.: A focussed look at the Alpine Fault, New Zealand: Seismicity, focal mechanisms, and stress observations, Journal of Geophysical Research, 106, 2193-2220, 2001.

Lindroos, Z. R.: Microstructures Developed during Creep Deformation of Quartz: an Investigation of Shape and Crystallographic Characteristics, M. Sc., Geology Department, University of Otago, Dunedin, New Zealand, 119 pp., 2013.

Little, T., Holcombe, R. J., and Ilg, B. R.: Ductile fabrics in the zone of active oblique convergence near the Alpine Fault, New Zealand: identifying the neotectonic overprint, Journal of Structural Geology, 24, 193-217, 2002a.

Little, T. A.: Transpressive ductile flow and oblique ramping of lower crust in a two-sided orogen: Insight from quartz grain-shape fabrics near the Alpine fault, New Zealand, Tectonics, 23, doi:10.1029/2002TC001456, 2004.

Little, T. A., Cox, S., Vry, J. K., and Batt, G.: Variations in exhumation level and uplift rate along the obliqu-slip Alpine fault, central Southern Alps, New Zealand, Geological Society of America Bulletin, 117, 707-723, 2005.

Little, T. A., Holcombe, R. J., and Ilg, B. R.: Kinematics of oblique collision and ramping inferred from microstructures and strain in middle crustal rocks, central Southern Alps, New Zealand, Journal of Structural Geology, 24, 219-239, 2002b.

Little, T. A., Prior, D. J., and Toy, V. G.: Are quartz LPOs predictably oriented with respect to the shear zone boundary?: A test from the Alpine Fault mylonites, New Zealand, Geochemistry Geophysics Geosystems, 981-999, doi:10.1002/2015GC006145, 2016.

Little, T. A., Prior, D. J., Toy, V. G., and Lindroos, Z. R.: The link between strength of lattice preferred orientation, second phase content and grain boundary migration: A case study from the Alpine Fault zone, New Zealand, Journal of Structural Geology, 59-77, doi:10.1016/j.jsg.2015.09.004 2015.

Liu, Z. and Bird, P.: Finite element modeling of neotectonics in New Zealand, Journal of Geophysical Research, 107, doi:10.1029/2001JB001075, 2002.

MacRae, C. M., Wilson, N. C., and Torpy, A.: Hyperspectral cathodoluminescence, Mineralogy and Petrology, 107, 429-440, doi:10.1007/s00710-013-0272-8, 2013.

Menzies, C. D., Teagle, D. A. H., Craw, D., Cox, S. C., Boyce, A. J., Barrie, C. D., and Roberts, S.: Incursion of meteoric waters into the ductile regime in an active orogen, Earth and Planetary Science Letters, 2014, 1-13, doi:10.1016/j.epsl.2014.04.046, 2014.

Nachlas, W. and Hirth, G.: Experimental constraints on the role of dynamic recrystallization on resetting the Ti-in-quartz thermobarometer, Journal of Geophysical Research, 120, doi:10.1002/2015JB012274, 2015.

Nachlas, W., Whitney, D., Teyssier, C., Bagley, B., and Mulch, A.: Titanium concentration in quartz as a record of multiple deformation mechanisms in an extensional shear zone, Geochemistry Geophysics Geosystems, 15, 1374-1397, doi:10.1002/2013GC005200, 2014.

Nevitt, J. M., Warren, J. M., Kidder, S., and Pollard, D. D.: Comparison of thermal modeling, microstructural analysis, and Ti-in-quartz thermobarometry to constrain the thermal history of a cooling pluton during deformation in the Mount Abbot Quadrangle, CA, Geochemistry Geophysics Geosystems, 18, 1270-1297, doi:10.1002/2016GC006655, 2017.

Niemeijer, A. R., Boulton, C., V. G., T., Townend, J., and Sutherland, R.: Large-displacement, hydrothermal frictional properties of DFDP-1 fault rocks, Alpine Fault, New Zealand: Implications for deep rupture propagation, Journal of Geophysical Research: Solid Earth, 624-647, doi:10.1002/ 2015JB012593, 2016.

Norris, R. and Cooper, A.: The Alpine Fault, New Zealand: Surface Geology and Field Relationships, American Geophysical Union, 157-175, doi:10.1029/175GM09, 2007.

Norris, R. and Toy, V.: Continental transforms: A view from the Alpine Fault, Journal of Structural Geology, 64, 3-31, doi:10.1016/j.jsg.2014.03.003, 2014.

Norris, R. J. and Cooper, A. F.: Very high strains recorded in mylonites along the Alpine Fault, New Zealand: implications for the deep structure of plate boundary faults, Journal of Structural Geology, 25, 2141-2157, 2003.

Shi, Y. L., Allis, R., and Davey, F.: Thermal modeling of the Southern Alps, New Zealand, Pure and Applied Geophysics, 146, 469-501, 1996.

Sibson, R. H.: Fault rocks and fault mechanisms, Journal of the Geological Society of London, 133, 191-213, 1977.

Sibson, R. H., White, S. H., and Atkinson, B. K.: Fault rock distribution and structure within he Alpine Fault Zone: A Preliminary Account, Royal Society of New Zealand Bulletin, 18, 55-65, 1979.

Sibson, R. H., White, S. H., and Atkinson, B. K.: Structure and distribution of fault rocks in the Alpine Fault Zone, New Zealand, Geological Society of London Special Publication, 9, 1981.

Spear, F. S.: Metamorphic phase equilibria and pressure-temperature-time paths, Mineralogical Society of America, Washington, D.C., 1995.

Spear, F. S., Ashley, K. T., Webb, L. E., and Thomas, J. B.: Ti diffusion in quartz inclusions: implications for metamorphic time scales, Contributions to Mineralogy and Petrology, doi:10.1007/s00410-012-0783-z, 2012.

Stern, T., Okaya, D., Kleffmann, S., Scherwath, M., Henrys, S., and Davey, F.: Geophysical Exploration and Dynamics of the Alpine Fault Zone, A Continental Plate Boundary: Tectonics at South Island, New Zealand doi:10.1029/175GM11, 2007.

Stipp, M., Stünitz, H., Heilbronner, R., and Schmid, S. M.: Dynamic recrystallization of quartz: correlation between natural and experimental conditions, Geol Soc Spec Publ, 200, 171-190, 2002.

Stöckhert, B., Brix, M. R., Kleinschrodt, R., Hurford, A. J., and Wirth, R.: Thermochronometry and microstructures of quartz - a comparison with experimental flow laws and predictions on the temperature of the brittle-plastic transition, Journal of Structural Geology, 21, 351-369, 1999.

Sutherland, R., Davey, F., and Beavan, J.: Plate boundary deformation in South Island, New Zealand, is related to inherited lithospheric structure, Earth and Planetary Science Letters, 177, 141-151, 2000.

Sutherland, R., Eberhart-Phillips, D., Harris, R. A., Stern, T., Beavan, J., Ellis, S., Henrys, S., cox, S., norris, R., Berryman, K., Townend, J., Bannister, S., Pettinga, J., Leitner, B., Wallace, L., Little, T., cooper, A. F., Yetton, M., and Stirling, M.: Do Great Earthquakes occur on the Alpine Fault in central South Island, new Zealand? In: A Continental Plate Boundary: Tectonics at South Island, New Zealand, Geophysical Monograph Series 175, 2007.

Sutherland, R., Townend, J., Toy, V., Upton, P., Coussens, J., Allen, M., Baratin, L.-M., Barth, N., Becroft, L., Boese, C., Boles, A., Boulton, C., Broderick, N. G. R., Janku-Capova, L., Carpenter, B. M., Célérier, B., Chamberlain, C., Cooper, A., Coutts, A., Cox, S., Craw, L., Doan, M.-L., Eccles, J., Faulkner, D., Grieve, J., Grochowski, J., Gulley, A., Hartog, A., Howarth, J., Jacobs, K., Jeppson, T., Kato, N., Keys, S., Kirilova, M., Kometani, Y., Langridge, R., Lin, W., Little, T., Lukacs, A., Mallyon, D., Mariani, E., Massiot, C. c., Mathewson, L., Melosh, B., Menzies, C., Moore, J., Morales, L., Morgan, C., Mori, H., Niemeijer, A., Nishikawa, O., Prior, D., Sauer, K., Savage, M., Schleicher, A., Schmitt, D. R., Shigematsu, N., Taylor-Offord, S., Teagle, D., Tobin, H., Valdez, R., Weaver, K., Wiersberg, T., Williams, J., Woodman, N., and Zimmer, M.: Extreme hydrothermal conditions at an active plate-bounding fault, Nature, 546, 137-140, doi:10.1038/nature22355, 2017.

Sutherland, R., Toy, V. G., Townend, J., Cox, S. C., Eccles, J. D., Faulkner, D. R., Prior, D. J., Norris, R. J., Mariani, E., Boulton, C., Carpenter, B. M., Menzies, C. D., Little, T. A., Hasting, M., Pascale, G. P. D., Langridge, R. M., Scott, H. R., Reid, Z., Lindroos, Fleming, B., and Kopf, A. J.: Drilling reveals fluid control on architecture and rupture of the Alpine fault, New Zealand, Geology, 40, 1143-1146, doi:10.1130/G33614.1, 2012.

Thomas, J. B., Watson, E. B., Spear, F. S., Shemella, P. T., Nayak, S. K., and Lanzirotti, A.: TitaniQ under pressure: the effect of pressure and temperature on the solubility of Ti in quartz, Contributions to Mineralogy and Petrology, 160, 743-759, doi:10.1007/s00410-010-0505-3, 2010.

Thomas, J. B., Watson, E. B., Spear, F. S., and Wark, D. A.: TitaniQ recrystallized: experimental con rmation of the original Ti-in-quartz calibrations, Contributions to Mineralogy and Petrology, 169:27, doi:10.1007/s00410-015-1120-0, 2015.

Toy, V. G.: Rheology of the Alpine Fault Mylonite Zone: deformation processes at and below the base of the seismogenic zone in a major plate boundary structure, PhD, Geology Department, University of Otago, Dunedin, 629 pp., 2007.

Toy, V. G., Boulton, C. J., Sutherland, R., Townend, J., Norris, R. J., Little, T. A., Prior, D. J., Mariani, E., Faulkner, D., Menzies, C. D., Scott, H., and Carpenter, B. M.: Fault rock lithologies and architecture of the central Alpine fault, New Zealand, revealed by DFDP-1 drilling, Lithosphere, 7, 155-173, doi:10.1130/L395.1, 2015.

Toy, V. G., Craw, D., Cooper., A. F., and Norris, R. J.: Thermal regime in the central Alpine Fault zone, New Zealand: Constraints from microstructures, biotite chemistry, and fluid inclusion data, Tectonophysics, 485, 178-192, doi:10.1016/j.tecto.2009.12.013, 2010.

Toy, V. G., Norris, R. J., Prior, D. J., Walrond, A. F., and Cooper, A. F.: How do lineations reflect the strain history of transpressive shear zones? The example of the active Alpine Fault zone, New Zealand, Journal of Structural Geology, 50, 187-198, doi:10.1016/j.jsg.2012.06.006, 2013.

Toy, V. G., Prior, D. J., and Norris, R. J.: Quartz fabrics in the Alpine Fault mylonites: Influence of pre-existing preferred orientations on fabric development during progressive uplift, Journal of Structural Geology, 30, 602-621, 2008.

Toy, V. G., Prior, D. J., Norris, R. J., Cooper, A. F., and Walrond, M.: Relationships between kinematic indicators and strain during syn-deformational exhumation of an oblique slip, transpressive, plate boundary shear zone: The Alpine Fault, New Zealand, Earth and Planetary Science Letters, 333-334, 282-292, doi:10.1016/j.epsl.2012.04.037, 2012.

van Daalen, M., Heilbronner, R., and Kunze, K.: Orientation analysis of localized shear deformation in quartz fibres at the brittle-ductile transition, Tectonophysics, 303, 83-107, 1999.

Vry, J., Baker, J., Maas, R., Little, T. A., Grapes, R., and Dixon, M.: Zoned (Cretaceous and Cenozoic) garnet and the timing of high grade metamorphism, Southern Alps, New Zealand, Journal of Metamorphic Geology, 22, 137-157, doi:10.1111/j.1525-1314.2004.00504.x, 2004.

Vry, J. K., Powell, R., and Williams, J.: Establishing the P–T path for Alpine Schist, Southern Alps near Hokitika, New Zealand, Journal of Metamorphic Geology, 26, 81-97, 2007.

Walcott, R. I.: Present tectonics and late Cenozoic evolution of New Zealand, Reviews of Geophysics, 36, 1-26, 1998.

Wark, D. and Spear, F.: Ti in quartz: Cathodoluminescence and thermometry, Goldschmidt 2005, A592.

Wark, D. A. and Watson, B.: TitaniQ: a titanium-in-quartz geothermometer, Contributions to Mineralogy and Petrology, 2006, 743-754, 2006.

Table 1. Information on individual samples. All samples are from Gaunt Creek with the exception of Stony Creek sample ST-12c_iv. GPS data use the New Zealand Transverse Mercator Projection 2000. Distances are estimated structural distances measured perpendicular to foliation. Rutile and Chlorite columns indicate whether these minerals were observed (“y”) or not (“n”). Sample identified by numbers 77*** are archived in the Otago University collection.

Sample	**Northing**	**Easting**	**Distance (m)**	**Composition**	**Structure type**	**Rutile**	**Chlorite**
77921	5,200,537	1,382,891	83	qfs	mylonite	y	n
77911	5,200,537	1,382,891	118	qfs	mylonite	n	n
77920	5,200,511	1,383,128	133	mafic part	mylonite	y	trace
77920	5,200,511	1,383,128	133	chert part	mylonite	y	trace
77821	5,200,508	1,382,904	140	qfs/mafic	ultramylonite	y	y
77913	5,200,511	1,382,888	137	chert	mylonite	y	y
77915	5,200,511	1,382,888	137	mafic part	mylonite	y	y
77915	5,200,511	1,382,888	137	vein in mafic	mylonite	y	n
77923	5,200,516	1,383,157	149	mafic part	mylonite	y	y
77923	5,200,516	1,383,157	149	chert part	mylonite	y	n
77912	5,200,551	1,382,908	159	augen mafic feldspar	ultramylonite	n	y
77925	5,200,564	1,383,283	246	qfs	mylonite	y	n
77925	5,200,564	1,383,283	246	vein in qfs	mylonite	y	in late vein
77886	5,200,429	1,383,283	292	qfs	mylonite/proto	y	y
77887	5,200,426	1,383,287	293	mafic part	mylonite	n	n
77887	5,200,426	1,383,287	293	chert part	mylonite	y	y
77900	5,200,409	1,383,570	461	chert	schist	y	n
5.2.1.13	5,200,409	1,383,570	461	qfs	proto	n	n
5.26.1.18	5,200,409	1,383,570	461	qfs	proto	n	n
77930	5,200,362	1,383,619	515	mafic	proto	n	y
77932	5,200,344	1,383,638	541	mafic part	proto	y	n
77932	5,200,344	1,383,638	541	chert part	proto	y	n
05.2.1.11	5,200,344	1,383,638	541	qfs	proto	n	y
05.2.1.11	5,200,344	1,383,638	541	vein in qfs	proto	n	n
77878	5,200,202	1,383,798	741	qfs	proto/schist	y	y
ST-12c_iv	5,193,839	1,374,804	800	qfs	proto	n	y
77875	5,200,152	1,383,943	869	qfs	proto/schist	n	in vein
77982	5,200,115	1,384,037	942	qfs	schist	y	n
77980	5,200,163	1,384,269	1090	qfs	schist	y	y

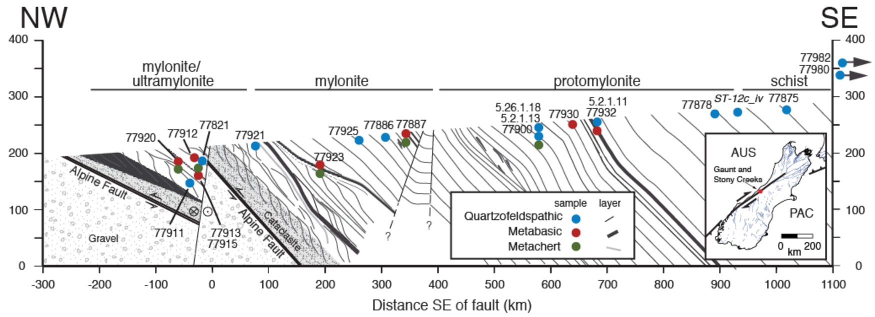

Figure 1. Schematic cross section of Gaunt Creek after Toy et al. (2008) showing approximate sample locations. Inset shows the S. Island of New Zealand and the locations of Gaunt and Stony creeks. The position of the the Stony Creek sample (ST-12c_iv) is projected into an approximate position based on its structural distance from the Alpine fault.

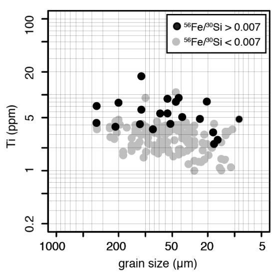

Figure 2. Plot of grain size vs. Ti showing all analyses where Fe was measured. Analyses with high Fe contents (^{56}Fe/^{30}Si ratios >0.007) are plotted in black. The coincidence of high Fe/Si ratios with high Ti suggests that the high Ti analyses were contaminated by some non-quartz phase, possibly Fe-Ti oxides which are common in the Alpine Fault mylonites. All analyses with ^{56}Fe/^{30}Si ratios >0.007 or Ti concentrations >5 ppm were removed from the dataset (see text for details).

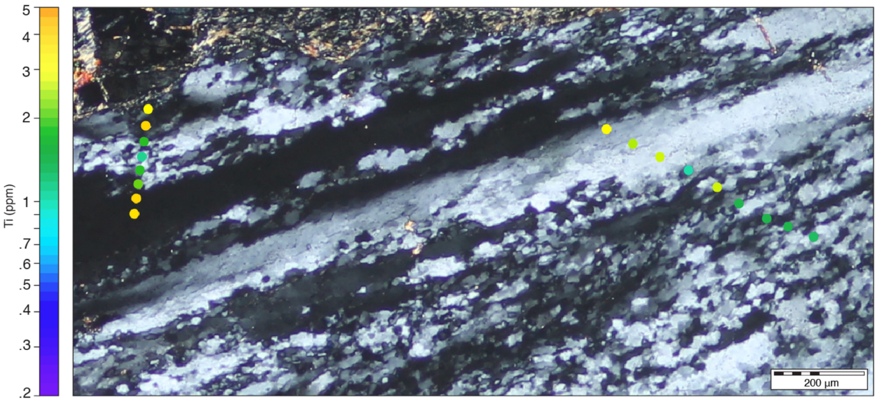

Figure 3. Cross polarized image showing dynamically recrystallized quartz in an ultramylonite sample (77912). Large ribbon grains, showing undulose extinction and subgrains, are interpreted as remnants, predating ultramylonite deformation. Recrystallized zones contain small, more equant grains with relatively uniform extinction. Typical of samples found within ~150 m of the Alpine Fault, lower Ti concentrations (green dots) are found in recrystallized zones than in the ribbon grains (yellow and orange dots).

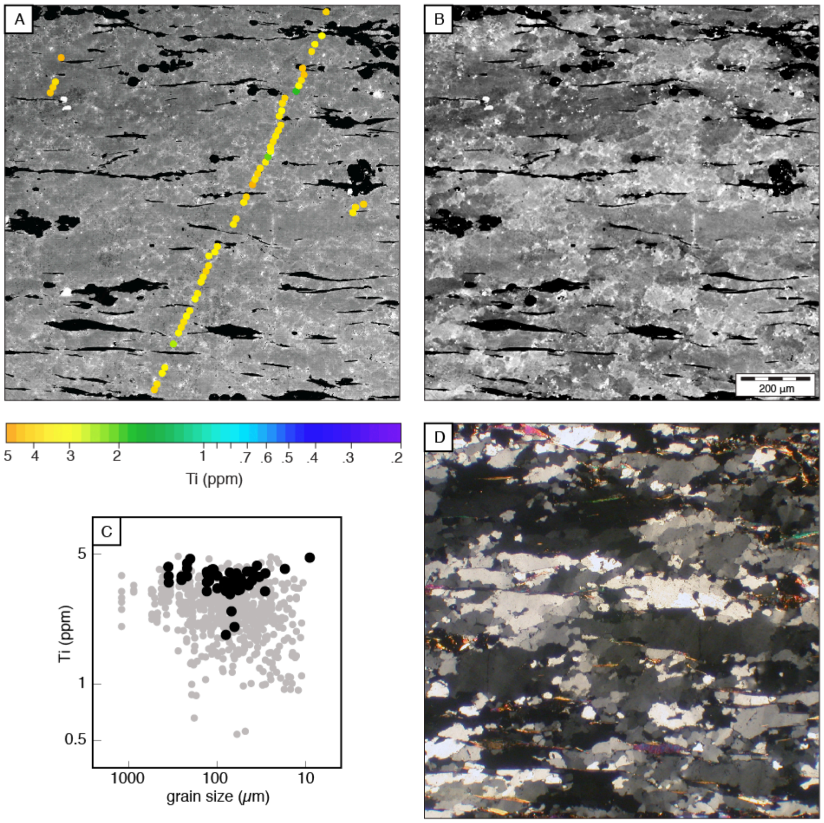

Figure 4. (A.) Panchromatic (200-960 nm) cathodoluminescence (CL) image of protomylonite metachert sample 77900 showing uniformity of Ti concentrations at analysis points. (B) 470 nm wavelength cathodoluminescence (CL) image. (C) Ti-in-quartz data for this sample (black) against a backdrop of data from other Gaunt Creek samples—no variation in Ti content with grain size is observed. (D) Cross-polarized photomicrograph of the same area. As typical of many samples, Ti-in-quartz contents vary between ~2 and 3 ppm, with no apparent spatial pattern. The blue spectrum peak (~470 nm, 2.65 eV) is dependent on quartz c-axis orientation, since dark grains in panel (B) are also dark in panel (D). The Ti peak at ~415 nm (Wark and Spear, 2005) was not detected in this sample, probably due to the low concentrations of Ti in the sample.

Deleted: correlates

Deleted: with

Deleted: such that

Deleted: grains with c-axes oriented perpendicular to the plane of the section are dark in panels (B) and (D)

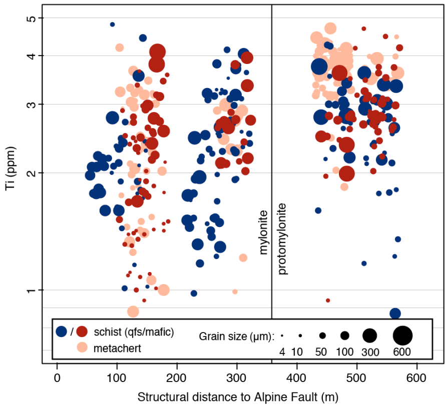

Figure 5. Ti concentrations vs. distance to the Alpine Fault, with analyses colored as a function of sample composition. With the exception of two protomylonite metachert samples with high Ti (at ~450 and 550 m), no systematic effect of composition is evident. Samples at structural distances >600 m are not plotted because they are uniformly quartzofeldspathic (qfs). The data are jittered along the x axis by an amount not exceeding 30 km in order to increase the visibility of the data.

Deleted: The data are jittered along the x-axis to increase visibility.

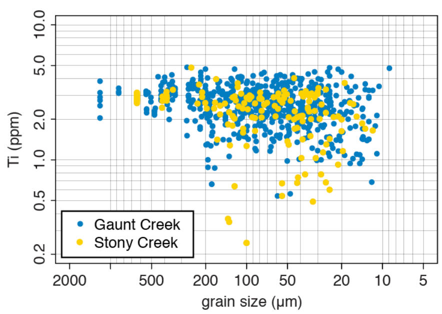

Figure 6. Plot of Ti concentration vs. grain size for all data. Grains >~250 µm have a relatively homogeneous Ti concentration ~2-4 ppm which we interpret to predate Alpine Fault deformation. Smaller grains (<200 µm) were at least partly formed by dynamic recrystallization during late stages of deformation, exhumation, and cooling. Despite very large strains (γ = 12-120) at high temperature, less than half of the small recrystallized grains have Ti concentrations significantly lower than relict values of 2-4 ppm. We interpret that most deformation was associated with pressure-temperature conditions where Ti concentrations of 2-4 ppm were stable, specifically that mylonite and protomylonite deformation occurred along a cooling path that followed a constant-Ti isopleth (see text for details). Stony Creek analyses include data from Cross et al (2015).

Deleted: grain size

Deleted: Ti concentration

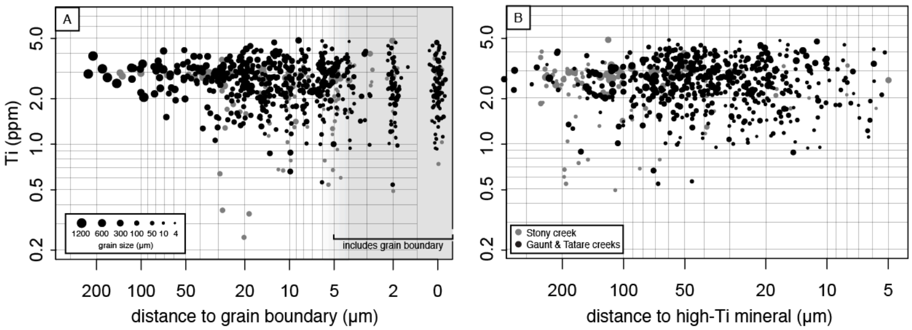

Figure 7. Ti concentrations in quartz vs. the distance (in thin section plane) from the analysis center to the nearest (A) grain boundary (of any type) or (B) dark mineral that might act as a potential Ti source or sink such as biotite or Fe-Ti-oxide. The increased presence of low Ti concentrations closer to grain boundaries (panel A) results from recrystallization and diffusion during deformation at decreasing temperatures. The lack of a clear trend in (B) suggests that Ti-in-quartz concentrations were not strongly affected by proximity to neighboring Ti-rich phases and that diffusion of Ti along grain boundaries was not a limiting factor in Ti-in-quartz concentrations. Data from Cross et al. (2015) are plotted in panel A but are not available for panel B. The data are jittered along the x axis in order to increase visibility.

Deleted: The lack of low Ti quartz (<1 ppm) within 50 µm of high-Ti minerals (B) may relate to a locally elevated Ti activity in the immediate vicinity of such minerals at low temperatures.

Deleted: The data are jittered along the x axis to increase visibility.

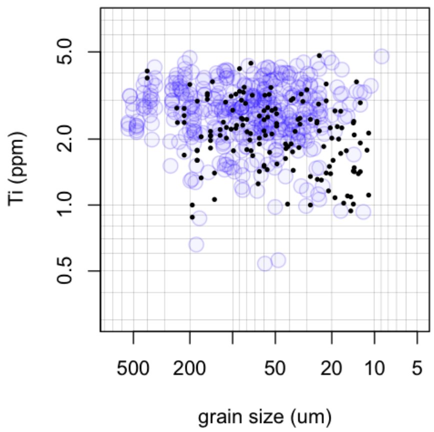

Figure 8. Ti vs. grain size for Gaunt Creek samples. Samples at structural distances <160 m from the fault are shown in black (mainly ultramylonites), while mylonites and protomylonites are plotted in transparent purple. The trend in the samples close to the fault suggests late recrystallization (as indicated by finer grain size) occurred at conditions where lower concentrations of Ti were stable. Only partial equilibration of Ti-in-quartz values was achieved during recrystallization of fine grains in the ultramylonite. Away from the fault there is not a general trend of fine grains having lower Ti concentrations.”

Deleted: Grain size vs. Ti for Gaunt Creek samples. Samples at structural distances <160 m from the fault are shown in black (mainly ultramylonites), while mylonites and protomylonites are plotted in transparent purple. The trend in the samples close to the fault suggests late recrystallization occurred at lower temperatures (with variable resetting). Away from the fault this trend is not observed—grain sizes tend to be larger, Ti tends to be greater, and, although it may occur in some samples, there is not a general trend of fine grains having lower Ti concentrations. In the ultramylonites, however, lower Ti concentrations (1-2 ppm) appear to have been stable during recrystallization of the finer grains. We interpret that deformation of the protomylonites and mylonites occurred during cooling that closely followed a Ti-isopleth (~2-4 ppm) in pressure-temperature space (e.g. Figure 11), but that ultramylonite deformation occurred at pressure-temperature conditions where Ti values of 1-2 ppm were stable. Only partial equilibration of Ti-in-quartz values was achieved during recrystallization of fine grains in the ultramylonite.

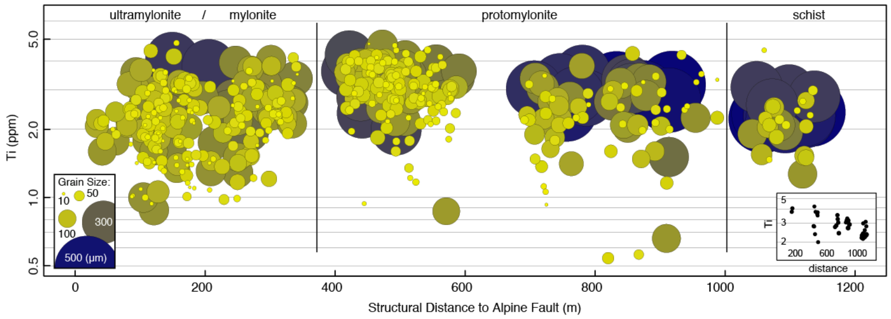

Figure 9. Ti concentrations vs. distance from the Alpine fault for Gaunt Creek samples, with dot size indicating grain size. Small recrystallized grains (<~300 µm) near the fault are more likely to show decreased Ti concentrations than similar sized recrystallized grains away from the fault—this supports microstructural observations (e.g. Fig. 3) that lower Ti concentrations were stable during ultramylonite deformation but not during mylonite and protomylonite deformation. Inset shows Ti concentration in the coarsest grains (>300 µm) increases slightly towards the fault. The data are jittered along the x axis by an amount not exceeding 50 km in order to increase visibility.

Deleted: ure

Deleted: Data are jittered along the x-axis

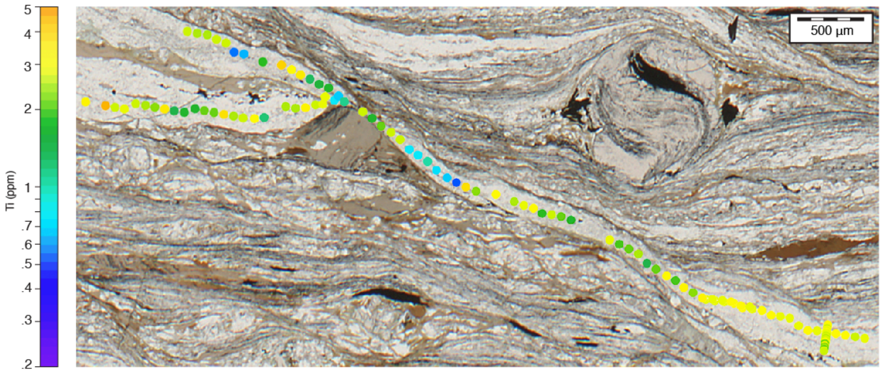

Figure 10. Photomicrograph of an older foliation (near horizontal in this image) cut by a C’ shear band in a sample from Stony Creek. Ti concentrations are plotted from both inside and outside the shear band. Most of the lowest Ti measurements are from within the shear band, indicating some loss of Ti in quartz recrystallized during formation of the C’ layer. The foliations preserved in the garnet (upper right) and large biotite grain predate Alpine Fault deformation.

Deleted: Image

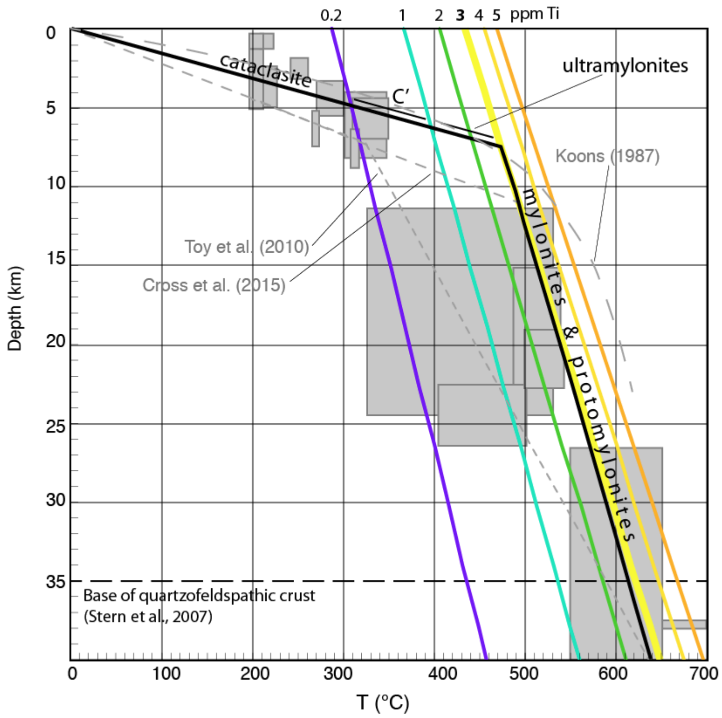

Figure 11. Temperature-depth diagram showing constraints on the Alpine Fault geothermal gradient from previous studies (grey boxes), proposed and previously proposed geothermal gradients (solid black and dashed lines, respectively), and experimentally determined constant-Ti contours (colored "isopleths") covering the range of observed Ti-in-quartz concentrations. A Ti activity of 0.1 (Thomas et al., 2010) and crustal density of 2.7 g/cm^3 are used to plot the isopleths. Ti activity is constrained by the fact that activities larger than 0.1 would shift the isopleths to the left and require quartz recrystallization at unrealistically low quartz recrystallization temperatures (<300 °C). Previous temperature-pressure constraints are from Craw (1997), Holm et al. (1989), Green (1992), Grapes (1995), Cooper (1980), and Vry et al. (2004) as summarized by Toy et al. (2010).

Deleted: The geothermal gradient proposed here is based on new data indicating mylonite and protomylonite deformation occurred at temperatures from roughly 600 to 450 °C whilst Ti-in-quartz concentrations of ~3 ppm were stable.

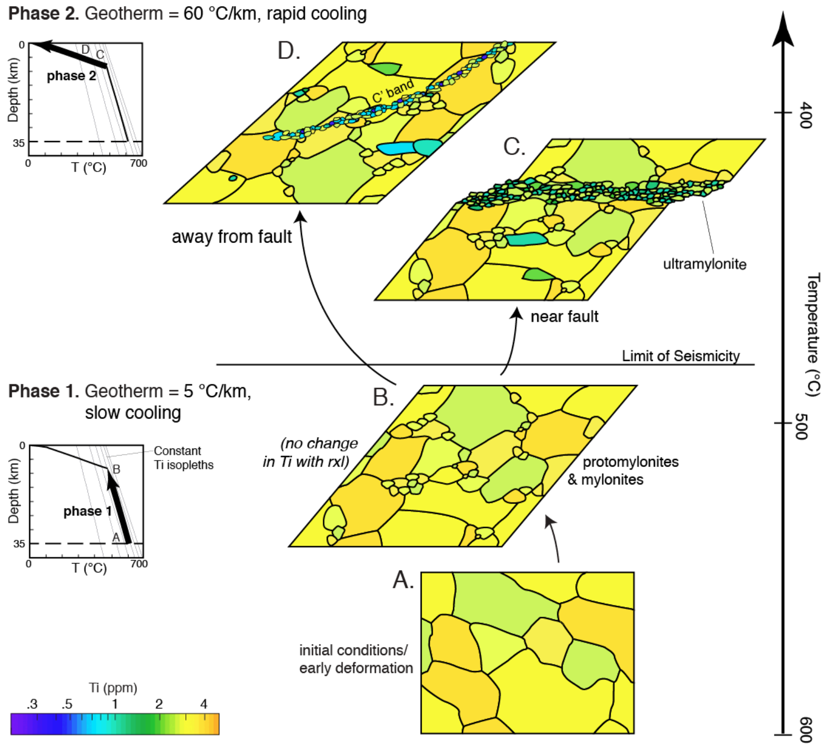

Figure 12. Simplified illustration of interpreted microstructural and Ti-in-quartz evolution. "Phase 1" deformation begins with Ti-in-quartz concentrations at 2-4 ppm (A). Strain associated with protomylonite and mylonite formation (B) involves recrystallization with no change in Ti-in-quartz concentrations due to exhumation along a constant-Ti isopleth (e.g. Fig. 11). During "phase 2," newly recrystallized quartz grains tend to have lower Ti concentrations as a result of cooling along a much steeper segment of the geothermal gradient (Fig. 11). Near the fault (C), ultramylonites form with Ti-in-quartz concentrations of 1-2 ppm. The latest quartz recrystallization occurs away from the fault in protomylonites and mylonites in C' bands (D). Sporadic recrystallization of some medium-sized grains with Ti-in-quartz concentrations below 2 ppm occurs in some rocks during phase 2.

Deleted: ure

Deleted: ure